INSTITUTE OF PHYSICS PUBLISHING INVERSE PROBLEMS

Inverse Problems **20** (2004) 1455–1478 PII: S0266-5611(04)73834-4

Inversion of the 3D exponential parallel-beam transform and the Radon transform with angle-dependent attenuation

Leonid A Kunyansky

Department of Mathematics, University of Arizona, Tucson, AZ 85721, USA

E-mail: leonk@math.arizona.edu

Received 29 December 2003, in final form 21 May 2004
Published 27 July 2004
Online at stacks.iop.org/IP/20/1455
doi:10.1088/0266-5611/20/5/008

Abstract

The inversion problem for the 3D parallel-beam exponential ray transform is solved through inversion of a set of the 2D exponential Radon transforms with complex-valued angle-dependent attenuation. An inversion formula for the latter 2D transform is derived; it generalizes the known Kuchment–Shneiberg formula valid for real angle-dependent attenuation. We derive an explicit theoretically exact solution of the 3D problem which is valid for arbitrary closed trajectory that does not intersect itself. A simple reconstruction algorithm is described, applicable for certain sets of trajectories satisfying Orlov's condition. In the latter case, our inversion technique is as stable as the Tretiak–Metz inversion formula. Possibilities of further reduction of noise sensitivity are briefly discussed in the paper. The work of our algorithm is illustrated by an example of image reconstruction from two circular orbits.

1. Introduction

Single photon emission computed tomography (SPECT) is based on measurements of the intensity of gamma rays emitted by a radiotracer injected into the patient's blood. The goal of SPECT is to reconstruct the position-dependent activity of the tracer from the data acquired by a set of collimated detectors moving around the patient. The measured values are proportional to the weighted line integrals from the activity. To make reconstruction possible, one has to collect measurements over a 3D set of lines passing through the body. The SPECT reconstruction problem we consider is a generalization of that arising in traditional x-ray tomography. For both kinds of tomography the simplest reconstruction techniques are obtained when the measurement directions are parallel to a plane, and each set of measurements contains data acquired for parallel rays. In this case (independently of the type of radiation used), the 3D reconstruction problem naturally decomposes into a set of independent 2D

problems, whose theory and inversion techniques are currently well understood (see, e.g., [11–15] for 2D SPECT reconstruction techniques).

However, the quest for more efficient measurement strategies has led to the use of non-planar measurement orbits and non-parallel beam acquisition schemes. The problems of x-ray tomography arising from more complex acquisition geometries have been extensively and successfully studied (the related references are too numerous to list here). One of the first results obtained by Orlov [10] in 1975 pertains to the case of the parallel-beam measurements. When this kind of data acquisition is utilized, one set of measurements (a projection) consists of the values of integrals taken along lines parallel to a fixed vector. It is convenient to represent the latter vector by a point on a sphere of directions $\mathbb{S}^2$. Orlov [10] has shown that the reconstruction is possible if each great circle on $\mathbb{S}^2$ contains at least one measurement direction. (A great circle is the intersection of $\mathbb{S}^2$ with a plane passing through its centre.)

In this paper, we investigate the problem of SPECT reconstruction from parallel-beam data. One of the complications of SPECT (as compared to x-ray tomography) is related to the presence of exponential weights in the integrals modelling propagation of gamma photons through the absorbing tissue. Most of the recent results on SPECT reconstruction from the data measured from non-planar and/or non-parallel directions (obtained from the fan-beam or cone-beam acquisition schemes) either consider the case when the measurement directions contain a great circle [1, 3] or require computation of certain Neumann series converging to the exact solution [2].

The only known general and theoretically exact approach is described in [4] (see also [5]). Work [4] considers the case of a rotating slant-hole (RSH) detector which measures parallel-beam projections from the set of directions represented by a circle (other than a great one). The authors process the data using an ingenious exact rebinning procedure based on the formula [9] which allows one to reconstruct absent measurements corresponding to the arbitrary directions contained within the circle. Interestingly, the attenuation corresponding to the reconstructed measurements does not have to coincide with the physical attenuation in the tissues, and can even be set to zero, although such a choice somewhat reduces the stability of the method. In order to collect a sufficient amount of data for the full 3D reconstruction, several measurement circles are positioned in such a way that the union of the interiors of all the circles covers some great circle. Then, using the re-binning procedure, one reconstructs absent measurements corresponding to directions lying on the great circle and the problem reduces to the case of planar measurements. Depending on the value of the artificial attenuation used to generate absent measurements, the 3D problem is solved by inverting a set of 2D either exponential or classical Radon transforms. In the classical case, when artificial attenuation was set to zero, it is sufficient to collect data covering only 180° angular range, i.e., only a half of the great circle. Further, the reb-inning algorithm can be easily generalized [6] to the case of arbitrary closed non-self-intersecting 1D sets of measurement directions (other than circles).

In this paper, we propose a different approach to explicit 3D reconstruction from the parallel-beam data measured along closed non-self-intersecting 1D trajectories, in the presence of constant attenuation. By the use of the 1D Fourier transform we reduce the 3D problem to a set of 2D exponential Radon transforms with angle-dependent complex-valued attenuation (AD-ERT). The latter 2D transforms can be explicitly inverted by application of the Kuchment–Shneiberg formula [9] generalized to the case of complex-valued attenuation. Such an approach results in a set of explicit reconstruction formulae; these formulae hold regardless of whether Orlov's condition is satisfied or not. A simple analysis of the operations involved in such an inversion shows that if Orlov's condition is not satisfied, a stable numerical reconstruction of certain spatial frequencies is not possible. In the simplest case of a circular

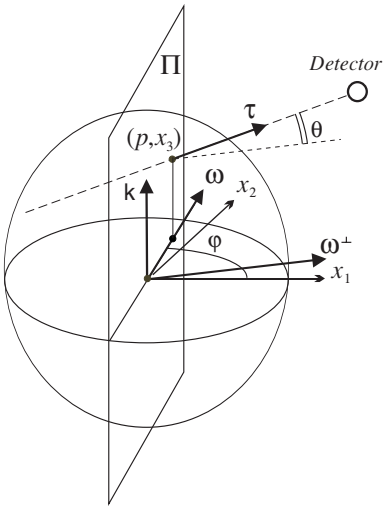

Figure 1. Geometry of the data acquisition scheme.

measurement trajectory, only frequencies lying outside a certain cone can be recovered in a stable fashion.

In order to obtain a stable 3D reconstruction one can combine two sets of measurements from sufficiently wide circular orbits (or, more generally, from two closed non-self-intersecting trajectories satisfying certain conditions). We present a simple reconstruction algorithm for such a data acquisition scheme; performance of this method is further illustrated by a computational example.

2. Formulation of the problem

We seek to recover the 3D radioactivity distribution $F(\mathbf{r})$ from the values of radiation intensity measured by a collimated parallel-beam detector sensitive only to gamma photons propagating in a selected direction. A single projection (a 2D set of measurements) consists of the intensity values for each ray passing through the body and parallel to τ, see figure 1. Since $F(\mathbf{r})$ is a function of three spatial variables one has to obtain a 3D set of data to reconstruct it. A natural way to gather such data is to conduct measurements from directions τ varying along continuous 1D trajectories. We parametrize each direction $\tau(\varphi, \theta)$ by the elevation angle θ and azimuthal angle φ. In sections 2–5 we restrict our consideration to such trajectories that can be described by a continuous function $\theta = \theta(\varphi), \varphi \in [0, 2\pi]$, with bounded piece-wise continuous derivative; we assume that the trajectory is closed, i.e., $\theta(2\pi) = \theta(0)$, and that $|\theta| < \pi/2$. The latter inequality guarantees that the trajectory does not intersect itself. In section 6, we will consider a case when a second measured trajectory is added, also described by the equation $\theta' = \theta'(\varphi')$ but in a coordinate system rotated in space in a certain way.

Let us introduce a rotating coordinate system $(\varpi(\varphi), \varpi^{\perp}(\varphi), \mathbf{k})$:

$$\varpi(\varphi) = (\cos\varphi, \sin\varphi, 0), \qquad \varpi^{\perp}(\varphi) = (\sin\varphi, -\cos\varphi, 0), \qquad \mathbf{k} = (0, 0, 1).$$

Each line of measurement in a single projection is uniquely defined by coordinates (p, x_3) of the point of intersection between the line and the plane Π spanned by vectors $\varpi(\varphi)$ and $\mathbf{k}$, see figure 1. We assume that the attenuation ν is constant. Then, the intensity of the radiation

$G(p, \varphi, x_3)$ leaving the body along the line passing through the point (p, x_3), in the direction $\tau(\varphi, \theta(\varphi))$, is related to the activity $F(\mathbf{r})$ by the equation

$$G(p, \varphi, x_3) = \int_{t_1(p,\varphi,x_3)}^{t_2(p,\varphi,x_3)} F[p\varpi(\varphi) + x_3\mathbf{k} + t\tau(\varphi, \theta(\varphi))]\, \mathrm{e}^{\nu(t-t_2(p,\varphi,x_3))}\, \mathrm{d}t, \tag{1}$$

where $t_1(p, \varphi, x_3)$, $t_2(p, \varphi, x_3)$ are the points at which the line intersects the boundary of the body. The above equation represents a simplified mathematical model of measurements; it takes into account absorption of gamma photons on its way to the detector, but neglects effects of the photon scatter, quantum noise and detector blur.

If the contour of the body is known and is convex, equation (1) can be reduced [7] to the exponential ray transform (ERT) as follows:

$$G^{\mathrm{ERT}}(p, \varphi, x_3) = G(p, \varphi, x_3)\, \mathrm{e}^{\nu t_2(p,\varphi,x_3)} = \int_{\mathbb{R}} F[p\varpi(\varphi) + x_3\mathbf{k} + t\tau(\varphi, \theta(\varphi))]\, \mathrm{e}^{\nu t}\, \mathrm{d}t. \tag{2}$$

Otherwise, if the shape of the body is unknown, the consistency conditions for the ERT can be used to find the scaling coefficients (see [8]) and thus complete the reduction. We assume throughout the paper that the modified projections $G^{\mathrm{ERT}}(p, \varphi, x_3)$ are given.

(Note that our parametrization of the data is slightly non-standard. Usually the plane defining the origin $t = 0$ of the integration variable is chosen to be perpendicular to the direction of measurement. In our case this plane (Π) is vertical. One of the consequences of such parametrization is that the projections $G^{\mathrm{ERT}}(p, \varphi, x_3)$ differ from a standard definition by a known exponential factor $\mathrm{e}^{x_3 \sin\theta(\varphi)}$. We choose this parametrization because it makes the problem invariant to the shift in the $\mathbf{k}$-direction, and thus simplifies its Fourier analysis.)

Our goal is to reconstruct $F(\mathbf{r})$ from the projections $G^{\mathrm{ERT}}(p, \varphi, x_3)$ assuming that the latter are known for a certain continuous set of directions $\tau(\varphi, \theta(\varphi))$. First, we will consider the case of a single closed trajectory $\theta = \theta(\varphi)$, with φ varying from 0 to 2π. As shown in the next section, then the problem can be theoretically solved by inverting a set of 2D exponential Radon transforms with complex-valued angle-dependent attenuation (AD-ERT). We analyse several explicit inversion formulae for the latter transform in section 4. The discussion of the original 3D problem resumes in section 6, where we show that in order to obtain a numerically stable reconstruction, one may need to supplement one-orbit measurements by the second set of measurements.

3. Reduction to the 2D exponential Radon transform with complex angle-dependent attenuation

As mentioned in the previous section, under the chosen parametrization the problem becomes invariant to the vertical shift. We will use this fact to decompose the 3D formulation into a set of independent 2D problems. To this end let us introduce a new variable of integration $s = t\cos\theta(\varphi)$, and express τ as a linear combination of $\varpi^{\perp}(\varphi)$ and $\mathbf{k}$:

$$\tau(\varphi, \theta(\varphi)) = \varpi^{\perp}(\varphi)\cos\theta(\varphi) + \mathbf{k}\sin\theta(\varphi),$$

so that equation (2) can be re-written as

$$\begin{aligned} G^{\mathrm{ERT}}(p, \varphi, x_3)\cos\theta(\varphi) &= \int_{\mathbb{R}} F[p\varpi + s\varpi^{\perp} + \mathbf{k}(x_3 + s\tan\theta(\varphi))]\, \mathrm{e}^{s\nu/\cos\theta(\varphi)}\, \mathrm{d}s \\ &= \int_{\mathbb{R}} F^*[p\varpi + s\varpi^{\perp}, x_3 + s\tan\theta(\varphi)]\, \mathrm{e}^{s\nu/\cos\theta(\varphi)}\, \mathrm{d}s \end{aligned} \tag{3}$$

where $F(\mathbf{r}) = F^*(\mathbf{x}, x_3)$ with $\mathbf{x} = (x_1, x_2, 0)$, $\mathbf{r} = \mathbf{x} + x_3\mathbf{k}$. Function $F^*(\mathbf{x}, x_3)$ is related to its 1D Fourier transformant $f(\mathbf{x}, \xi_3)$ by the formula

$$F(\mathbf{r}) = F^*(\mathbf{x}, x_3) = \frac{1}{\sqrt{2\pi}} \int_{\mathbb{R}} f(\mathbf{x}, \xi_3)\, \mathrm{e}^{\mathrm{i}x_3\xi_3}\, \mathrm{d}\xi_3. \tag{4}$$

By substituting (4) into (3) we obtain

$$\begin{aligned} G^{\mathrm{ERT}}(p, \varphi, x_3)\cos\theta(\varphi) &= \frac{1}{\sqrt{2\pi}} \int_{\mathbb{R}} \left[\int_{\mathbb{R}} f(p\varpi + s\varpi^{\perp}, \xi_3)\, \mathrm{e}^{\mathrm{i}(x_3 + s\tan\theta(\varphi))\xi_3}\, \mathrm{d}\xi_3 \right] \mathrm{e}^{sv/\cos\theta(\varphi)}\, \mathrm{d}s \\ &= \frac{1}{\sqrt{2\pi}} \int_{\mathbb{R}} \left[\int_{\mathbb{R}} f(p\varpi + s\varpi^{\perp}, \xi_3)\, \mathrm{e}^{s(\mathrm{i}\xi_3\tan\theta(\varphi) + v/\cos\theta(\varphi))}\, \mathrm{d}s \right] \mathrm{e}^{\mathrm{i}x_3\xi_3}\, \mathrm{d}\xi_3. \end{aligned} \tag{5}$$

Finally, taking the 1D Fourier transform from both sides of equation (5) one arrives at the following formula:

$$g(p, \varphi, \xi_3) = \int_{\mathbb{R}} f[p\varpi(\varphi) + s\varpi^{\perp}(\varphi), \xi_3]\, \mathrm{e}^{(v/\cos\theta(\varphi) + \mathrm{i}\xi_3\tan\theta(\varphi))s}\, \mathrm{d}s \tag{6}$$

where

$$g(p, \varphi, \xi_3) \equiv \frac{1}{\sqrt{2\pi}} \int_{\mathbb{R}} G^{\mathrm{ERT}}(p, \varphi, x_3)\cos\theta(\varphi)\, \mathrm{e}^{-\mathrm{i}x_3\xi_3}\, \mathrm{d}x_3. \tag{7}$$

Now, by introducing the notation

$$\mu(\varphi) \equiv v/\cos\theta(\varphi) + \mathrm{i}\xi_3\tan\theta(\varphi), \tag{8}$$

one can re-write equation (6) in the form

$$g_{\xi_3}(p, \varphi) = \int_{\mathbb{R}} f[p\varpi(\varphi) + s\varpi^{\perp}(\varphi), \xi_3]\, \mathrm{e}^{\mu(\varphi)s}\, \mathrm{d}s. \tag{9}$$

For each fixed value of the parameter ξ_3 the above equation can be viewed as the 2D exponential Radon transform with a complex-valued angle-dependent attenuation (AD-ERT). The (non-physical) complex attenuation $\mu(\varphi)$ in (9) arises due to the particular technique we used to simplify the original 3D problem; obviously, it does not coincide with the physical real-valued attenuation v.

In the following section, explicit formulae are presented for the inversion of the AD-ERT (9) for an arbitrary value of ξ_3. These formulae allow one to obtain an explicit expression for $f(\mathbf{x}, \xi_3)$ in terms of the Fourier transform $g(p, \varphi, \xi_3)$ of the projections $G^{\mathrm{ERT}}(p, \varphi, x_3)\cos\theta(\varphi)$. Solution $F^*(\mathbf{x}, x_3)$ of the 3D problem under consideration is then computed using equation (4). It is worth mentioning that, since $F(\mathbf{r})$ is a real-valued function, in the numerical implementations of this method only values of $f(\mathbf{x}, \xi_3)$ for $\xi_3 \geqslant 0$ have to be computed due to the equality $f(\mathbf{x}, -\xi_3) = \overline{f(\mathbf{x}, \xi_3)}$.

In the next section, we discuss in detail inversion formulae for the 2D AD-ERT; these formulae will be used in section 6 to complete the analysis of the 3D problem at hand.

4. Inversion of the 2D AD-ERT

As was shown in the previous section, the full 3D reconstruction problem can be solved by inverting a set of the 2D AD-ERT (9) for each real value of the parameter ξ_3. In this section, we present inversion formulae for the latter 2D transform. In order to simplify notation we assume that ξ_3 is given and fixed, and we omit this parameter throughout this section. Thus, our goal is to invert the AD-ERT in the following form:

$$g(p, \varphi) = \int_{\mathbb{R}} f[p\varpi(\varphi) + s\varpi^{\perp}(\varphi)]\, \mathrm{e}^{\mu(\varphi)s}\, \mathrm{d}s. \tag{10}$$

4.1. Kuchment–Shneiberg's inversion formula

In 1994, a set of explicit formulae was obtained by Kuchment and Shneiberg [9] for inversion of the AD-ERT (10) in the presence of real angle-dependent attenuation $\mu(\varphi)$. These formulae have an important practical application as an integral part of the 3D reconstruction technique of [4, 5]. We reproduce below the simplest of the Kuchment–Shneiberg formulae proposed in [9], in a slightly modified notation. The formula is of the filtration-backprojection (FBP) type: it combines linear filtration $\Lambda_{\mu(\varphi)}$ of the projections $g(p,\varphi)$

$$(\Lambda_{\mu(\varphi)}g)(p,\varphi) = \mathcal{F}^{-1}[\hat{\eta}(\rho,\varphi)\hat{g}(\rho,\varphi)] \tag{11}$$

with the exponential backprojection $B_{\mu(\varphi)}$ defined for an arbitrary function $u(p,\varphi)$ as follows:

$$(B_{\mu(\varphi)}u(p,\varphi))(\mathbf{x}) = \frac{1}{2\pi}\int_0^{2\pi} u(\mathbf{x}\cdot\varpi(\varphi),\varphi)\,\mathrm{e}^{-\mu(\varphi)(\mathbf{x}\cdot\varpi^{\perp}(\varphi))}\,\mathrm{d}\varphi. \tag{12}$$

In (11), $\hat{g}(\rho,\varphi)$ is the 1D Fourier transform of $g(p,\varphi)$ in the first variable

$$\hat{g}(\rho,\varphi) \equiv (\mathcal{F}g)(\rho,\varphi) = \frac{1}{\sqrt{2\pi}}\int_{\mathbb{R}} g(p,\varphi)\,\mathrm{e}^{-\mathrm{i}\rho p}\,\mathrm{d}p, \tag{13}$$

and symbol $\mathcal{F}^{-1}$ stands for the inverse Fourier transform. The filter $\hat{\eta}(\rho,\varphi)$ used in (11) is given by the expression

$$\hat{\eta}(\rho,\varphi) = \begin{cases} \frac{|\rho|}{2}\left(1 - \frac{\mathrm{i}\mu'(\varphi)}{\rho}\right), & |\rho| > \mu(\varphi) \\ 0, & |\rho| < \mu(\varphi). \end{cases} \tag{14}$$

The composition of the filtration and exponential backprojection yields the desired reconstruction

$$f(\mathbf{x}) = (B_{\mu(\varphi)}\Lambda_{\mu(\varphi)}g)(\mathbf{x}). \tag{15}$$

The validity of the explicit reconstruction technique described by equations (11)–(15) was proven in [9] by application of the Cauchy theorem in $\mathbb{C}^2$. A proof based on application of the Cauchy theorem in $\mathbb{C}^1$ was later given in [6].

4.2. Inversion formulae for complex-valued attenuation

For the purposes of this paper we need to invert AD-ERT with complex-valued attenuation. We derive such an inversion formula in section 5 by obtaining a slice-projection theorem in polar coordinates, in a form containing complex-valued angles, and by applying the Cauchy theorem in $\mathbb{C}^1$. Our derivation generalizes the proof presented in [6]. Although such an approach is less elegant than the approach of [9], it is more accessible to a wider engineering audience, and it also yields some additional insight, necessary for the construction of efficient numerical algorithms. The formula we present is valid under the assumption that $f(\mathbf{x})$ is a continuous finitely supported function with a bounded piece-wise continuous gradient. We will need to assume that $f(\mathbf{x})$ is a complex-valued function, since it was originally introduced as the Fourier transform of another function, see equation (4). We also assume that $\mu(\varphi)$ is a continuous complex-valued periodic function of φ with bounded piece-wise continuous derivative. This requirement is satisfied, for example, if $\mu(\varphi)$ is defined by equation (8) in which function $\theta(\varphi)$ describes a trajectory satisfying the restrictions formulated in the beginning of section 3. Finally, under the above assumptions projection $g(p,\varphi)$ is a continuous function of both arguments; moreover, for each fixed φ the derivative $\frac{\mathrm{d}}{\mathrm{d}p}g(p,\varphi)$ is a piece-wise continuous function.

Similarly to (15), our FBP-type inversion formula can be written in the form

$$f(\mathbf{x}) = \left(B_{\mu(\varphi)}\Lambda^{\text{present}}_{\mu(\varphi)}g\right)(\mathbf{x}). \tag{16}$$

The above expression is a composition of the conventional weighted backprojection (12) with the new filtration operation $\Lambda^{\text{present}}_{\mu(\varphi)}$ that modifies a given continuous compactly supported function $u(p)$ with a bounded piece-wise continuous derivative as follows:

$$\left(\Lambda^{\text{present}}_{\mu(\varphi)} u\right)(p) = \frac{1}{2\sqrt{2\pi}} \int_{\Gamma^-_{\mu(\varphi)}+\Gamma^+_{\mu(\varphi)}} \hat{u}(z)\, \mathrm{e}^{\mathrm{i}pz}\, \Delta(z,\varphi) z\, \mathrm{d}z, \tag{17}$$

$$\Delta(z,\varphi) = 1 - \mathrm{i}\mu'(\varphi)/z. \tag{18}$$

The integration contour in the above integral consists of two oriented arcs, Γ^+_μ and Γ^-_μ. The shape of these two arcs varies for different projections; it depends on the value of $\mu(\varphi)$. In detail, arc Γ^+_μ is defined by the equation

$$z = t + \mathrm{i}\frac{1}{t}\mu_R\mu_I, \qquad \mu_R \leqslant t \leqslant \infty, \tag{19}$$

where

$$\mu_R \equiv \operatorname{Re}\mu, \qquad \mu_I \equiv \operatorname{Im}\mu,$$

and the starting point of the arc corresponds to $t = \mu_R$. Arc Γ^-_μ is equal to $-\Gamma^+_\mu$. The Fourier transform $\hat{u}(z)$ in (17) is well defined for complex values of z due to the finite support of $u(p)$. Obviously, the above new filtration procedure contains equations (11)–(14) as a particular case corresponding to purely real $\mu(\varphi)$.

A different inversion formula for the case of complex-valued $\mu(\varphi)$ can be obtained by modifying the original Kuchment–Shneiberg formula. The only obstacle for a straightforward generalization of formulae (11), (12) and (14) is the inequalities in (14) which do not make sense in the case of complex $\mu(\varphi)$. However, there is an easy way around. Let us replace filtration procedure (11), (14) by an equivalent operator

$$\left(\Lambda^{\text{Novikov}}_{\mu(\varphi)} u\right)(p) = \frac{1}{4}\left(\frac{\mathrm{d}}{\mathrm{d}p} + \mu'(\varphi)\right)\{\mathrm{e}^{-\mathrm{i}\mu p}\mathcal{H}[\mathrm{e}^{\mathrm{i}\mu p}u(p)] + \mathrm{e}^{\mathrm{i}\mu p}\mathcal{H}[\mathrm{e}^{-\mathrm{i}\mu p}u(p)]\}, \tag{20}$$

where $\mathcal{H}$ stands for the Hilbert transform

$$(\mathcal{H}u)(p) = \frac{1}{\pi}\int_{-\infty}^{\infty} \frac{u(s)}{p-s}\, \mathrm{d}s.$$

Although the original work of Novikov [15] does not consider the case of the angle-dependent attenuation, the above operator (20) is rather similar to the one appearing in Novikov's inversion formula when attenuation is constant (see [15, 16]). We thus use notation $\Lambda^{\text{Novikov}}_{\mu(\varphi)}$ to refer to the filtration procedure (20). The equivalence of Λ_μ and $\Lambda^{\text{Novikov}}_\mu$ for purely real $\mu(\varphi)$ is easy to verify, for example, by slightly modifying analysis of section 4 in [16]. Since the formula

$$f(\mathbf{x}) = \left(B_{\mu(\varphi)}\Lambda^{\text{Novikov}}_{\mu(\varphi)} g\right)(\mathbf{x}) \tag{21}$$

is valid for real-valued $\mu(\varphi)$, and since all the operators involved depend on μ analytically, one can conjecture that formula (21) is also valid for complex-valued $\mu(\varphi)$. We show in the next section that inversion formulae (21) and (16) are equivalent. This fact, in particular, can serve as a formal proof of the Kuchment–Shneiberg formula in the form (21) for complex $\mu(\varphi)$.

4.3. Equivalence of the two inversion formulae

It is not difficult to prove that the two inversion operators defined by equations (21) and (16), respectively, are equivalent when applied to projections $g(p,\varphi)$. Indeed, since the backprojection parts of these two formulae are exactly the same, in order to prove our assertion

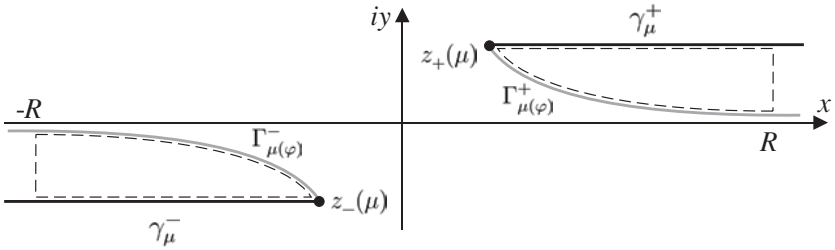

Figure 2. Integration paths $\Gamma_\mu^\pm$ and $\gamma_\mu^\pm$.

it is enough to verify equivalence of the filtration operators (17) and (20). To this end, we first modify the expression in braces in (20) as follows:

$$\begin{aligned}&\mathrm{e}^{-\mathrm{i}\mu p}\mathcal{H}[\mathrm{e}^{\mathrm{i}\mu p}u(p)] + \mathrm{e}^{\mathrm{i}\mu p}\mathcal{H}[\mathrm{e}^{-\mathrm{i}\mu p}u(p)]\\ &\qquad = \mathrm{e}^{-\mathrm{i}\mu p}\{(\mathcal{H}+\mathrm{i}\mathcal{I})[u(p)\,\mathrm{e}^{\mathrm{i}\mu p}]\}(p) + \mathrm{e}^{\mathrm{i}\mu p}\{(\mathcal{H}-\mathrm{i}\mathcal{I})[u(p)\,\mathrm{e}^{-\mathrm{i}\mu p}]\}(p),\end{aligned} \tag{22}$$

where $\mathcal{I}$ is the identity operator. The action of the operator $\mathcal{H}-\mathrm{i}\mathcal{I}$ on some function $v(p)$ can be expressed in terms of the Fourier transform of v

$$[(\mathcal{H}-\mathrm{i}\mathcal{I})v]\,(p) = \mathcal{F}^{-1}\{(-\mathrm{i}\,\mathrm{sign}\,\rho-\mathrm{i})\hat{v}(\rho)\}(p) = -\frac{2\mathrm{i}}{\sqrt{2\pi}}\int_0^{+\infty}\hat{v}(\rho)\,\mathrm{e}^{\mathrm{i}p\rho}\,\mathrm{d}\rho.$$

Therefore, taking into account that

$$\widehat{u(p)\,\mathrm{e}^{-\mathrm{i}\mu p}}(\rho) = \hat{u}(\rho+\mu)$$

we can re-write (22) as

$$\mathrm{e}^{\mathrm{i}\mu p}\{(\mathcal{H}-\mathrm{i}\mathcal{I})[u(p)\,\mathrm{e}^{-\mathrm{i}\mu p}]\}(p) = \frac{-2\mathrm{i}}{\sqrt{2\pi}}\int_0^{\infty}\hat{u}(\rho+\mu)\,\mathrm{e}^{\mathrm{i}p(\rho+\mu)}\,\mathrm{d}\rho. \tag{23}$$

Similarly, one obtains the identity

$$\mathrm{e}^{-\mathrm{i}\mu p}\{(\mathcal{H}+\mathrm{i}\mathcal{I})[u(p)\,\mathrm{e}^{\mathrm{i}\mu p}]\}(p) = \frac{-2\mathrm{i}}{\sqrt{2\pi}}\int_0^{-\infty}\hat{u}(\rho-\mu)\,\mathrm{e}^{\mathrm{i}p(\rho-\mu)}\,\mathrm{d}\rho. \tag{24}$$

Now, taking into account equations (23) and (24), filtration operator $\Lambda^{\text{Novikov}}_{\mu(\varphi)}$ (equation (20)) can be re-cast in the form of the following integral operator:

$$\begin{aligned}\left(\Lambda^{\text{Novikov}}_{\mu(\varphi)}u\right)(p) &= \frac{1}{2\sqrt{2\pi}}\int_{\gamma^-_{\mu(\varphi)}+\gamma^+_{\mu(\varphi)}}\hat{u}(z)\,\mathrm{e}^{\mathrm{i}pz}[z-\mathrm{i}\mu'(\varphi)]\,\mathrm{d}z\\ &= \frac{1}{2\sqrt{2\pi}}\int_{\gamma^-_{\mu(\varphi)}+\gamma^+_{\mu(\varphi)}}\hat{u}(z)\,\mathrm{e}^{\mathrm{i}pz}\Delta(z,\varphi)\,\mathrm{d}z\end{aligned} \tag{25}$$

where oriented arc γ_μ^+ is defined by

$$\gamma_\mu^+ : z = t+\mu, \qquad 0 \leqslant t < \infty, \tag{26}$$

with the starting point $z_+(\mu) = z(0) = \mu$. Arc γ_μ^- is defined as $\gamma_\mu^- = -\gamma_\mu^+$. The expressions representing the filtration operators (17) and (25) differ only by the integration contours. In both cases, the integration arcs $\gamma^\pm_{\mu(\varphi)}$ and $\Gamma^\pm_{\mu(\varphi)}$ start at the same points $z_\pm(\mu(\varphi)) = \pm\mu(\varphi)$ and go towards infinity within the strips $0 \leqslant y \leqslant \mu_I(\varphi)$ and $-\mu_I(\varphi) \leqslant y \leqslant 0$, respectively, see figure 2. The integrand in (17) and (25) is an entire function due to the finite support of $u(z)$. One can also show (see appendix for the details) that this integrand vanishes uniformly in y (within the strips) as $|\mathrm{Re}\,z|$ goes to infinity. Consider closed contours (shown by the dashed line in figure 2) generated by segments of integration arcs $\gamma^\pm_{\mu(\varphi)}$ and $\Gamma^\pm_{\mu(\varphi)}$ and lines

$\operatorname{Re} z = \pm R$. The integrals of $\hat{u}(z)\,\mathrm{e}^{\mathrm{i}pz}\Delta(z,\varphi)$ along each of the closed contours are equal to zero, and the integrals along vertical segments of these contours vanish in the limit $R \to \infty$. Therefore, the values of integrals (17) and (25) coincide, and inversion formulae (16) and (21) are equivalent when applied to projections $g(p,\varphi)$.

5. Derivation of the inversion formula

In order to derive the inversion formula given by equations (16)–(18) we will utilize a special form of the slice-projection theorem, presented in the next section. Using this result, in section 5.2 we develop a circular-harmonic reconstruction (CHR) algorithm. Then, as explained in section 5.3, the sought FBP-type inversion formula is easily obtained by integration over all spatial frequencies obtained from the CHR approach.

5.1. The slice-projection theorem

In this section, we analyse the relation between the Fourier transforms of function f and projections g, also known as the slice-projection theorem. For a fixed angle φ the slice-projection theorem in its simplest form does not differ from the corresponding relation for the constant attenuation case (see, for example, [11, 12]). Indeed, let us compute the 1D Fourier transform in p of a projection $g(p,\varphi)$ for an arbitrary complex value of spectral parameter z:

$$\begin{aligned}\hat{g}(z,\varphi) &= \frac{1}{\sqrt{2\pi}}\int_{-\infty}^{\infty}\left(\int_{\mathbb{R}} f[p\varpi(\varphi)+t\varpi^{\perp}(\varphi)]\,\mathrm{e}^{\mu(\varphi)t}\,\mathrm{d}t\right)\mathrm{e}^{-\mathrm{i}pz}\,\mathrm{d}p\\ &= \frac{1}{\sqrt{2\pi}}\int_{-\infty}^{\infty}\int_{-\infty}^{\infty} f(p\varpi+t\varpi^{\perp})\,\mathrm{e}^{t\mu(\varphi)-\mathrm{i}pz}\,\mathrm{d}t\,\mathrm{d}p.\end{aligned}$$

Noting that $t = \varpi^{\perp}\cdot\mathbf{x}$ and $p = \varpi\cdot\mathbf{x}$, we obtain

$$\begin{aligned}\hat{g}(z,\varphi) &= \frac{1}{\sqrt{2\pi}}\int_{\mathbb{R}^2} f((\varpi\cdot\mathbf{x})\varpi+(\varpi^{\perp}\cdot\mathbf{x})\varpi^{\perp})\,\mathrm{e}^{\mu\mathbf{x}\cdot\varpi^{\perp}-\mathrm{i}z\mathbf{x}\cdot\varpi}\,\mathrm{d}\mathbf{x}\\ &= \frac{1}{\sqrt{2\pi}}\int_{\mathbb{R}^2} f(\mathbf{x})\,\mathrm{e}^{-\mathrm{i}\xi(\mu,z,\varphi)\cdot\mathbf{x}}\,\mathrm{d}\mathbf{x} = \sqrt{2\pi}\,\hat{f}(\xi(\mu,z,\varphi))\end{aligned} \tag{27}$$

where

$$\xi(\mu,z,\varphi) = z\varpi(\varphi)+\mathrm{i}\mu(\varphi)\varpi^{\perp}(\varphi), \tag{28}$$

and $\hat{f}(\xi)$ is the 2D Fourier transform of $f(\mathbf{x})$:

$$\hat{f}(\xi) \equiv (\mathcal{F}_2 f)(\xi) = \frac{1}{2\pi}\int_{\mathbb{R}^2} f(\mathbf{x})\,\mathrm{e}^{-\mathrm{i}\xi\cdot\mathbf{x}}\,\mathrm{d}\mathbf{x}. \tag{29}$$

Equation (27) represents the slice-projection theorem in its simplest form. Note that even for purely real values of μ, equation (27) yields the values of the Fourier transform $\hat{f}$ corresponding to the complex-valued frequencies $\xi(\mu,z,\varphi)$.

For further use we need a polar-coordinate version of the slice-projection theorem, in which the frequencies are defined by a vector with a real-valued amplitude but whose direction is described by complex-valued angles. For the case of real-valued μ and z such a formula was derived in [11]; here we need a generalization of that result for the complex-valued attenuation.

Note that we have freedom of choice of the frequency z, due to the fact that each projection is finitely supported, and its Fourier transform is an entire function of z. Our task will be simplified if we utilize only those values of z that result in the orthogonality of the real and imaginary components of $\xi(\mu,z,\varphi)$. It is easy to see that the condition

$$\operatorname{Re}\xi(\mu,z,\varphi)\cdot\operatorname{Im}\xi(\mu,z,\varphi) = 0,$$

for $\xi(\mu, z, \varphi)$ defined by equation (28) is satisfied if $\operatorname{Im} z = \mu_R\mu_I/\operatorname{Re} z$. Thus, we will restrict our attention only to the values of z satisfying the equation

$$z = z(\rho, \mu) = \rho + \mathrm{i}\frac{\mu_R\mu_I}{\rho}. \tag{30}$$

Now we will cast $\xi(\mu, z, \varphi)$ in the form of a vector of a real length pointing in a complex direction. To this end $\operatorname{Re}\xi(\mu, z, \varphi)$ is transformed as follows:

$$\operatorname{Re}\xi(\mu, z, \varphi) = \rho\varpi(\varphi) - \mu_I\varpi^{\perp}(\varphi) = \operatorname{sign}(\rho)\sqrt{\rho^2 + \mu_I^2}\begin{pmatrix}\cos(\varphi + A(\rho, \mu_I))\\ \sin(\varphi + A(\rho, \mu_I))\end{pmatrix},$$

with angle $A(\rho, \mu_I) = \arctan\frac{\mu_I}{\rho}$. Similarly,

$$\operatorname{Im}\xi(\mu, z, \varphi) = \frac{\mu_R}{\rho}\operatorname{sign}(\rho)\sqrt{\rho^2 + \mu_I^2}\begin{pmatrix}\sin(\varphi + A(\rho, \mu_I))\\ -\cos(\varphi + A(\rho, \mu_I))\end{pmatrix}.$$

For $|\rho| > |\mu_R|$, the first component ξ_1 of vector $\xi(\mu, z, \varphi) = \operatorname{Re}\xi(\mu, z, \varphi) + \mathrm{i}\operatorname{Im}\xi(\mu, z, \varphi)$ can be re-cast in the following form:

$$\begin{aligned}\xi_1(\mu, z, \varphi) &= \operatorname{sign}(\rho)\frac{1}{\rho}\sqrt{\rho^2 + \mu_I^2}\,[\rho\cos(\varphi + A(\rho, \mu_I)) + \mathrm{i}\mu_R\sin(\varphi + A(\rho, \mu_I))]\\ &= \frac{1}{\rho}\sqrt{\rho^2 + \mu_I^2}\sqrt{\rho^2 - \mu_R^2}\cos(\varphi + A(\rho, \mu_I) - \mathrm{i}B(\rho, \mu_R))\\ &= \sigma(\rho, \mu)\cos\alpha(\rho, \mu, \varphi),\end{aligned}$$

where we introduced the following notation:

$$B = B(\rho, \mu_R) = \operatorname{arctanh}\frac{\mu_R}{\rho}, \tag{31}$$

$$\sigma(\rho, \mu) = \frac{1}{\rho}\sqrt{\rho^2 + \mu_I^2}\sqrt{\rho^2 - \mu_R^2}, \tag{32}$$

$$\alpha(\rho, \mu, \varphi) = \varphi + A(\rho, \mu_I) - \mathrm{i}B(\rho, \mu_R). \tag{33}$$

The second coordinate $\xi_2(\mu, z, \varphi)$ can be transformed in a similar way, which results in the equation

$$\xi(\mu, z(\rho, \mu), \varphi) = \sigma(\rho, \mu)\begin{pmatrix}\cos\alpha(\rho, \mu, \varphi)\\ \sin\alpha(\rho, \mu, \varphi)\end{pmatrix}. \tag{34}$$

Thus, a slice-projection theorem holds in the form

$$\hat{g}\left(\rho + \mathrm{i}\frac{\mu_R\mu_I}{\rho}, \varphi\right) = \sqrt{2\pi}\,\hat{f}^{\text{polar}}\left(\sigma(\rho, \mu), \alpha(\rho, \mu, \varphi)\right), \tag{35}$$

where $\hat{f}^{\text{polar}}(\sigma, \alpha)$ is the 2D Fourier transform of $f(\mathbf{x})$ in the polar coordinates (σ, α):

$$\hat{f}^{\text{polar}}(\sigma, \alpha) = \hat{f}\left(\xi(\sigma, \alpha)\right).$$

For further use, we obtain the following equation by representing $\mathbf{x} = (r\cos\theta, r\sin\theta, 0)$ in polar coordinates and using equations (28) and (34):

$$\begin{aligned}\mathbf{x}\cdot\xi(\mu, z(\rho, \mu), \varphi) &= z(\rho, \mu)\mathbf{x}\cdot\varpi(\varphi) + \mathrm{i}\mu(\varphi)\mathbf{x}\cdot\varpi^{\perp}(\varphi)\\ &= \sigma(\rho, \mu)r\cos(\alpha(\rho, \mu, \varphi) - \theta).\end{aligned} \tag{36}$$

For a fixed μ function, $\sigma(\rho, \mu)$ maps the domain $\Omega = \mathbb{R}\backslash[-\mu_R, \mu_R)$ onto $\mathbb{R}$. This mapping is bijective. Indeed, for $z = z(\rho, \mu)$ given by equation (30) the following identity holds true:

$$\sigma^2(\rho, \mu) = z^2(\rho, \mu) - \mu^2. \tag{37}$$

For a given σ this quadratic equation with respect to z has the unique solution

$$z^*(\sigma, \mu) = \sqrt{\sigma^2 + \mu^2}, \tag{38}$$

where the choice of the correct branch of the root is determined by the condition

$$\operatorname{sign}(\sigma) = \operatorname{sign}(\rho) = \operatorname{sign}(\operatorname{Re} z^*(\sigma, \mu)). \tag{39}$$

Obviously, the value of ρ corresponding to $z^*(\sigma, \mu)$ is $\rho^*(\sigma, \mu) = \operatorname{Re} z^*(\sigma, \mu)$.

Finally, for future reference we present the following expression for the angle $\alpha^*(\sigma, \varphi) = \alpha(\rho^*(\sigma, \mu), \mu, \varphi)$:

$$\alpha^*(\sigma, \varphi) = \varphi - \mathrm{i} \operatorname{arcsinh} \frac{\mu(\varphi)}{\sigma}, \tag{40}$$

which can be derived by means of simple trigonometric transformations

$$\begin{aligned} A(\rho, \mu_I) - \mathrm{i}B(\rho, \mu_R) &= \arctan \frac{\mu_I}{\rho} - \mathrm{i} \operatorname{arctanh} \frac{\mu_R}{\rho} \\ &= \arctan \frac{-\mathrm{i}\mu}{\rho + \mathrm{i}\frac{\mu_R \mu_I}{\rho}} = -\mathrm{i} \operatorname{arctanh} \frac{\mu}{z(\rho, \mu)} \\ &= -\mathrm{i} \operatorname{arcsinh} \frac{\mu}{\sigma(\rho, \mu)}. \end{aligned}$$

5.2. Reconstruction based on expansion in circular harmonics

Most of the advanced analytic algorithms for the inversion of the conventional exponential Radon transforms are based on expansions in circular harmonics (see [11, 13, 17–19]). Perhaps the most important advantage of such CHR algorithms is the improved stability of the reconstruction. (A general analysis of this property is given in [13].) A simple CHR algorithm for the inversion of AD-ERT can be obtained by combining the approach of [11] with the slice-projection theorem in the form (35), as explained below.

Let us expand $\hat{f}^{\text{polar}}(\sigma, \varphi)$ in the Fourier series in the angular variable:

$$\hat{f}_n(\sigma) = \frac{1}{2\pi} \int_0^{2\pi} \hat{f}^{\text{polar}}(\sigma, \varphi)\, \mathrm{e}^{-\mathrm{i}n\varphi}\, \mathrm{d}\varphi, \tag{41}$$

$$\hat{f}^{\text{polar}}(\sigma, \varphi) = \sum_{n=-\infty}^{\infty} \hat{f}_n(\sigma)\, \mathrm{e}^{\mathrm{i}n\varphi}. \tag{42}$$

Consider a fixed value of angle φ. For an arbitrary value of σ equations (38) and (40) provide values of $z^*(\sigma, \mu)$ and $\alpha^*(\sigma, \varphi)$ such that

$$\hat{g}(z^*(\sigma, \mu), \varphi) = \sqrt{2\pi}\, \hat{f}^{\text{polar}}(\sigma, \alpha^*(\sigma, \varphi)). \tag{43}$$

For each $\sigma > 0$, function $\hat{f}^{\text{polar}}(\sigma, \varphi)$ is the restriction of the Fourier transform $\hat{f}(\xi)$ to a real circle $|\xi| = |\sigma|, \operatorname{Im} \xi = 0$. Since f is finitely supported, $\hat{f}(\xi)$ is an entire function of 2D complex variable ξ. Therefore, for any fixed σ function $\hat{f}^{\text{polar}}(\sigma, \varphi)$ is entire in the angular variable, and is well defined for the complex values of the latter variable.

In order to compute $\hat{f}^{\text{polar}}(\sigma, \varphi)$ for real angular values it will suffice to find its Fourier coefficients $\hat{f}_n(\sigma)$. Due to analyticity of $\hat{f}^{\text{polar}}(\sigma, \varphi)$ in φ, the integration over the real interval $[0, 2\pi]$ in (41) can be replaced by integration over a closed arc C defined by equation $\alpha = \alpha^*(\sigma, \mu(\varphi), \varphi), 0 \leqslant \varphi \leqslant 2\pi$:

$$\begin{aligned} \hat{f}_n(\sigma) &= \frac{1}{2\pi} \oint_C \hat{f}^{\text{polar}}(\sigma, \alpha^*)\, \mathrm{e}^{-\mathrm{i}n\alpha^*}\, \mathrm{d}\alpha^* \\ &= \frac{1}{2\pi} \int_0^{2\pi} \hat{f}^{\text{polar}}(\sigma, \alpha^*(\sigma, \varphi))\, \mathrm{e}^{-\mathrm{i}n\alpha^*(\sigma,\varphi)} \frac{\partial}{\partial \varphi} \alpha^*(\sigma, \varphi)\, \mathrm{d}\varphi. \end{aligned}$$

Due to our assumptions on $\mu(\varphi)$, arc C is a rectifiable curve, and the above change of the integration contour is justified.

Values of $\hat{f}^{\text{polar}}(\sigma, \alpha^*)$ required by the last equation can be obtained from equation (43). We thus arrive at the reconstruction formula for $\hat{f}_n(\sigma)$:

$$\hat{f}_n(\sigma) = (2\pi)^{-\frac{3}{2}} \int_0^{2\pi} \hat{g}(z^*(\sigma, \mu), \varphi)\, \mathrm{e}^{-\mathrm{i}n\alpha^*(\sigma,\varphi)} \frac{\partial}{\partial\varphi}\alpha^*(\sigma, \varphi)\, \mathrm{d}\varphi. \tag{44}$$

The differentiation of $\alpha^*(\sigma, \varphi)$ yields

$$\frac{\partial}{\partial\varphi}\alpha^*(\sigma, \varphi) = 1 - \mathrm{i}\frac{\operatorname{sign}(\sigma)\mu'(\varphi)}{\sqrt{\sigma^2 + \mu^2(\varphi)}} = \left(1 - \mathrm{i}\frac{\mu'(\varphi)}{z^*(\sigma, \mu)}\right).$$

One can note that $\frac{\partial}{\partial\varphi}\alpha^*(\sigma, \varphi)$ coincides with the factor $\Delta(z^*(\sigma, \mu), \varphi)$ defined by equation (18). Now (44) can be re-written in the form

$$\hat{f}_n(\sigma) = (2\pi)^{-\frac{3}{2}} \int_0^{2\pi} \hat{g}(z^*(\sigma, \mu), \varphi)\, \mathrm{e}^{-\mathrm{i}n\alpha^*(\sigma,\varphi)} \Delta(z^*(\sigma, \mu), \varphi)\, \mathrm{d}\varphi. \tag{45}$$

This equation solves our reconstruction problem, since with $\hat{f}_n(\sigma)$ known $\hat{f}^{\text{polar}}(\sigma, \varphi)$ can be recovered by summing the Fourier series (42), and then $f(\mathbf{x})$ can be computed by the inverse Fourier transform.

The above derivation holds true also for negative values of σ, if one defines $\hat{f}^{\text{polar}}(-\sigma, \varphi) = \hat{f}^{\text{polar}}(\sigma, \varphi + \pi)$. This fact can be used to increase the stability of numerical implementation. Indeed, instead of $\hat{f}_n(\sigma)$ one can choose to reconstruct $\hat{f}_n(-\sigma)$ in view of the relation

$$\begin{aligned}\hat{f}_n(-\sigma) &= \frac{1}{2\pi}\int_0^{2\pi} \hat{f}^{\text{polar}}(-\sigma, \varphi)\, \mathrm{e}^{-\mathrm{i}n\varphi}\, \mathrm{d}\varphi \\ &= \frac{1}{2\pi}\int_0^{2\pi} \hat{f}^{\text{polar}}(\sigma, \varphi + \pi)\, \mathrm{e}^{-\mathrm{i}n\varphi}\, \mathrm{d}\varphi = (-1)^n \hat{f}_n(\sigma).\end{aligned}$$

The sign of the imaginary part of $\alpha^*(\sigma, \varphi)$ depends on the sign of σ, according to equations (31), (33) and (39); the sign of $\operatorname{Im}\alpha^*(\sigma, \varphi)$ in turn determines the sign of the real part of the expression $-\mathrm{i}n\alpha^*(\sigma, \varphi)$ in equation (45). If σ is positive, then $\operatorname{Re}(-\mathrm{i}n\alpha^*(\sigma, \varphi))$ is negative for positive n, and positive for negative n. While theoretically computation of $\hat{f}_n(\sigma)$ and $\hat{f}_n(-\sigma)$ is done in a similar manner, the sign of $\operatorname{Re}(-\mathrm{i}n\alpha^*(\sigma, \varphi))$ determines whether the exponent in equation (45) is smaller or greater than 1, which, in turn, affects the noise amplification properties of the algorithm. It is beneficial to compute $\hat{f}_n(\sigma)$ for $n \geqslant 0$ using positive σ, and find negative harmonics by computing $\hat{f}_n(-\sigma)$, $\sigma \geqslant 0, n < 0$. Such a regularizing technique is similar to the methods utilized in [11, 13, 17, 19] to reduce noise amplification in constant attenuation algorithms. In particular, one could generalize the approach of [11] to the case AD-ERT at hand. Such a method would consist in first recovering $\hat{f}_n(\sigma)$ as discussed above, then computing non-attenuated projections using a classical slice-projection theorem, and, finally, reconstructing $f(\mathbf{x})$ by backprojection of filtered (non-attenuated) projections. It is known that such an algorithm is significantly less unstable than Tretiak–Metz-like formulae described in the next section.

5.3. The FBP inversion formula

In this section, we use equation (45) to derive the FBP-type inversion formula given by equations (16)–(19).

Our assumptions on function $f(\mathbf{x})$ (see the beginning of section 4.2) allow us to express it through its inverse 2D Fourier transform in polar coordinates as follows:

$$f(\mathbf{x}(r,\psi)) = \frac{1}{2\pi}\int_0^{2\pi}\int_0^{\infty} \hat{f}^{\text{polar}}(\sigma,\varphi')\,\mathrm{e}^{\mathrm{i}\sigma r\cos(\varphi'-\psi)}\sigma\,\mathrm{d}\sigma\,\mathrm{d}\varphi'$$
$$= \frac{1}{2\pi}\int_0^{2\pi}\int_0^{\infty}\left[\sum_{n=-\infty}^{\infty}\hat{f}_n(\sigma)\,\mathrm{e}^{\mathrm{i}n\varphi'+\mathrm{i}\sigma r\cos(\varphi'-\psi)}\right]\sigma\,\mathrm{d}\sigma\,\mathrm{d}\varphi'. \qquad (46)$$

Let us introduce a mollified version $f^{N,R}(r,\psi)$ of $f(\mathbf{x}(r,\psi))$ defined by its truncated Fourier transform:

$$f^{N,R}(r,\psi) = \frac{1}{2\pi}\int_0^{2\pi}\int_0^{R}\left[\sum_{n=-N}^{N}\hat{f}_n(\sigma)\,\mathrm{e}^{\mathrm{i}n\varphi'+\mathrm{i}\sigma r\cos(\varphi'-\psi)}\right]\sigma\,\mathrm{d}\sigma\,\mathrm{d}\varphi'$$
$$= \frac{1}{2\pi}\int_0^{R}\int_0^{2\pi}\left[\sum_{n=-N}^{N}\hat{f}_n(\sigma)\,\mathrm{e}^{\mathrm{i}n\varphi'+\mathrm{i}\sigma r\cos(\varphi'-\psi)}\right]\mathrm{d}\varphi'\sigma\,\mathrm{d}\sigma.$$

Now we can substitute for $\hat{f}_n(\sigma)$ the right-hand side of equation (45), and change the integration order:

$$f^{N,R}(r,\psi) = (2\pi)^{-\frac{5}{2}}\int_0^{R}\int_0^{2\pi}$$
$$\times\left[\sum_{n=-N}^{N}\left(\int_0^{2\pi}\hat{g}(z^*,\varphi)\,\mathrm{e}^{-\mathrm{i}n\alpha^*}\Delta(z^*,\varphi)\,\mathrm{d}\varphi\right)\mathrm{e}^{\mathrm{i}n\varphi'+\mathrm{i}\sigma r\cos(\varphi'-\psi)}\right]\mathrm{d}\varphi'\sigma\,\mathrm{d}\sigma$$
$$= (2\pi)^{-\frac{5}{2}}\int_0^{R}\int_0^{2\pi}\hat{g}(z^*,\varphi)\Delta(z^*,\varphi)$$
$$\times\left[\sum_{n=-N}^{N}\left(\int_0^{2\pi}\mathrm{e}^{\mathrm{i}n\varphi'+\mathrm{i}\sigma r\cos(\varphi'-\psi)}\,\mathrm{d}\varphi'\right)\mathrm{e}^{-\mathrm{i}n\alpha^*}\right]\mathrm{d}\varphi\,\sigma\,\mathrm{d}\sigma,$$
$$z^* = z^*(\sigma,\mu), \qquad \alpha^* = \alpha^*(\sigma,\varphi).$$

The expression in brackets can be viewed as the Fourier series of $\mathrm{e}^{\mathrm{i}\sigma r\cos(\varphi'-\psi)}$ evaluated at the point $\varphi' = \alpha^*(\sigma,\varphi)$:

$$\lim_{N\to\infty}\frac{1}{2\pi}\sum_{n=-N}^{N}\left(\int_0^{2\pi}\mathrm{e}^{\mathrm{i}n\varphi'+\mathrm{i}\sigma r\cos(\varphi'-\psi)}\,\mathrm{d}\varphi'\right)\mathrm{e}^{-\mathrm{i}n\alpha^*(\sigma,\varphi)} = \mathrm{e}^{\mathrm{i}\sigma r\cos(\alpha^*(\sigma,\varphi)-\psi)}$$
$$= \mathrm{e}^{\mathrm{i}z^*(\sigma,\mu)\mathbf{x}\cdot\varpi(\varphi)-\mu(\varphi)\mathbf{x}\cdot\varpi^{\perp}(\varphi)}.$$

The last line in the above equation follows from (36). We thus obtain

$$f^{\infty,R}(\mathbf{x}) = \lim_{N\to\infty} f^{N,R}(r(\mathbf{x}),\psi(\mathbf{x}))$$
$$= (2\pi)^{-\frac{3}{2}}\int_0^{R}\int_0^{2\pi}\hat{g}(z^*(\sigma,\mu),\varphi)\Delta(z^*(\sigma,\mu),\varphi)\,\mathrm{e}^{\mathrm{i}z^*(\sigma,\mu)\mathbf{x}\cdot\varpi(\varphi)-\mu(\varphi)\mathbf{x}\cdot\varpi^{\perp}(\varphi)}\,\mathrm{d}\varphi\,\sigma\,\mathrm{d}\sigma.$$

Change of variables $z^*(\sigma,\mu)^2 = \sigma^2 + \mu^2(\varphi)$ yields

$$f^{\infty,R}(\mathbf{x}) = (2\pi)^{-\frac{3}{2}}\int_0^{2\pi}\int_{\Gamma^+(\mu(\varphi),R)}\hat{g}(z,\varphi)\,\mathrm{e}^{\mathrm{i}z\mathbf{x}\cdot\varpi(\varphi)-\mu(\varphi)\mathbf{x}\cdot\varpi^{\perp}(\varphi)}\Delta(z,\varphi)z\,\mathrm{d}z\,\mathrm{d}\varphi,$$

where the integration contour $\Gamma^+(\mu(\varphi), R)$ is defined by the equation $z = \sqrt{t^2 + \mu^2(\varphi)}$, $0 \leqslant t \leqslant R$, $\operatorname{Re} z > 0$. Now passing to the limit $R \to \infty$ we obtain

$$\begin{aligned} f(\mathbf{x}) &= \lim_{R\to\infty} f^{\infty,R}(\mathbf{x}) \\ &= (2\pi)^{-\frac{3}{2}} \int_0^{2\pi} \int_{\Gamma^+(\varphi,\infty)} \hat{g}(z,\varphi)\, \mathrm{e}^{\mathrm{i}z\mathbf{x}\cdot\varpi(\varphi) - \mu(\varphi)\mathbf{x}\cdot\varpi^\perp(\varphi)} \Delta(z,\varphi) z \,\mathrm{d}z \,\mathrm{d}\varphi \\ &= \frac{1}{2\pi} \int_0^{2\pi} \mathrm{e}^{-\mu(\varphi)\mathbf{x}\cdot\varpi^\perp(\varphi)} \left[\frac{1}{\sqrt{2\pi}} \int_{\Gamma^+(\mu(\varphi),\infty)} \hat{g}(z,\varphi)\, \mathrm{e}^{\mathrm{i}z\mathbf{x}\cdot\varpi(\varphi)} \Delta(z,\varphi) z \,\mathrm{d}z \right] \mathrm{d}\varphi. \end{aligned} \tag{47}$$

Comparing equations (30), (38) and (19) one can conclude that arc $\Gamma^+(\mu(\varphi), \infty)$ coincides with arc $\Gamma^+_{\mu(\varphi)}$ defined by equation (19). The inversion formula (47) can be viewed as the composition of the conventional weighted backprojection (see equation (12)) with the filtration operator $\Lambda^+_{\mu(\varphi)}$ defined by the expression in the brackets in equation (47), i.e.,

$$\left(\Lambda^+_{\mu(\varphi)} u\right)(p) = \frac{1}{\sqrt{2\pi}} \int_{\Gamma^+_{\mu(\varphi)}} \hat{u}(z)\, \mathrm{e}^{\mathrm{i}pz} \Delta(z,\varphi) z \,\mathrm{d}z. \tag{48}$$

A similar inversion formula in which filtration results from the integration over arc $\Gamma^+_{\mu(\varphi)}$ can be derived by defining $\hat{f}^{\text{polar}}(-\sigma,\varphi) = \hat{f}^{\text{polar}}(\sigma,\varphi+\pi)$ and setting 0 and $-\infty$ as the integration limits in the inner integral of equation (46). By repeating the derivation presented earlier in this section we arrive at the inversion formula

$$f(\mathbf{x}) = (B_{\mu(\varphi)} \Lambda^-_{\mu(\varphi)} g)(\mathbf{x}),$$

where $\Lambda^-_{\mu(\varphi)}$ is obtained by replacing $\Gamma^+_{\mu(\varphi)}$ with $\Gamma^-_{\mu(\varphi)}$ in equation (48). Alternatively, the use of the average $\Lambda^{\text{present}}_{\mu(\varphi)}$ of the two filtration operators

$$\Lambda^{\text{present}}_{\mu(\varphi)} = \tfrac{1}{2}\left(\Lambda^+_{\mu(\varphi)} + \Lambda^-_{\mu(\varphi)}\right). \tag{49}$$

combined with the weighted backprojection (12) also yields theoretically exact inversion. Equation (49) is equivalent to the filtration operator (17) presented in section 4.2. This completes our derivation of the inversion formulae (16) and (17).

5.4. Reconstruction with additional filtration

It is frequently desirable in computational practice to reconstruct the convolution $f^E(\mathbf{x})$ of the source term $f(\mathbf{x})$ with some distribution $E(\mathbf{x})$. The latter is usually defined by its Fourier transform $\hat{E}(\zeta)$, so that

$$f^E(\mathbf{x}) = \mathcal{F}_2^{-1}[\hat{E}(\zeta)\hat{f}(\zeta)](\mathbf{x}),$$

where ζ is the 2D vector dual to $\mathbf{x}$. It will suffice for the purposes of this paper to consider only rotationally symmetric filters $\hat{E}(\zeta) = \hat{E}(\sigma)$, $\sigma = |\zeta|$. By repeating the derivation of the previous section with $\hat{f}^{\text{polar}}(\sigma,\varphi')$ replaced by $\hat{E}(\sigma)\hat{f}^{\text{polar}}(\sigma,\varphi')$, one obtains the following equation:

$$f^E(\mathbf{x}) = \left(B_{\mu(\varphi)} \Lambda^E_{\mu(\varphi)} g\right)(\mathbf{x}),$$

where filtration operator $\Lambda^E_{\mu(\varphi)}$ contains an additional factor $\hat{E}(\sigma(z,\mu))$ under the integral:

$$\left(\Lambda^E_{\mu(\varphi)} u\right)(p) = \frac{1}{2\sqrt{2\pi}} \int_{\Gamma^+_{\mu(\varphi)} + \Gamma^-_{\mu(\varphi)}} \hat{u}(z)\, \mathrm{e}^{\mathrm{i}pz} \Delta(z,\varphi) \hat{E}(|\sigma^*(z,\mu)|) z \,\mathrm{d}z. \tag{50}$$

In the next section, we will need to use a particular kind of filtration that eliminates low spatial frequencies of a function. More precisely, we will utilize the filter $\hat{E}_M(|\sigma|)$ equal to 1

for $|\sigma| \geqslant M$ and equal to 0 otherwise. The use of this filter in (50) is equivalent to restricting the integration to the portions of the chain $\Gamma^+_{\mu(\varphi)} + \Gamma^-_{\mu(\varphi)}$ corresponding to $|\sigma| \geqslant M$. In other words, starting points $z^M_\pm$ of the truncated integration arcs are given by the condition

$$M^2 = \sigma^2 = z^2 - \mu^2(\varphi)$$

or $z^M_\pm(\mu(\varphi)) = \sqrt{M^2 + \mu^2(\varphi)}$, where $\operatorname{Re} z^M_+ > 0$ and $\operatorname{Re} z^M_- < 0$. We will use the notation $\Lambda^{\text{present}}_{\mu^M(\varphi)}$ to refer to this filtration operator.

The same effect can be achieved with the Novikov-style filtration procedure (equation (20) or, equivalently, (25)) if we replace $\mu(\varphi)$ by a modified value $\mu^M(\varphi) = z^M_+(\mu(\varphi))$. Indeed, the integration arcs in (25) will also start at the points $z^M_\pm(\mu(\varphi))$. Therefore, according to the analysis of section 4.3, the Novikov-style filtration procedure will yield the equivalent result. We will denote the corresponding operator by $\Lambda^{\text{Novikov}}_{\mu^M(\varphi)}$.

As explained in the next section, evaluation of the Fourier transform of a function for complex values of the frequencies leads to instabilities proportional to the imaginary part of the frequency. When filtration is done using operator $\Lambda^{\text{present}}_{\mu^M(\varphi)}$ (or equivalently, $\Lambda^{\text{Novikov}}_{\mu^M(\varphi)}$), the portions of the integration arcs with the largest values of $|\operatorname{Im} z|$ are eliminated, thus reducing the instability of the computation.

Assume, for simplicity, that $\mu(\varphi) = \mu$ does not depend on φ. (This situation corresponds to a circular measurement trajectory $\theta(\varphi) = \theta_0$ in the original 3D problem.) Given some number $K \geqslant 0$ we would like to find such a filtration operator that utilizes only those portions of $\Gamma^+_\mu + \Gamma^-_\mu$ for which $|\operatorname{Im} z| \leqslant K$. In view of equation (30), these parts of the path are described by the condition

$$|\rho| \geqslant |\mu_R \mu_I| / K. \tag{51}$$

If $|\mu_I| \leqslant K$ then this condition is automatically satisfied and no additional filtration is needed; all the range of frequencies σ is stably reconstructed. If $|\mu_I| > K$, then the range of the reconstructed frequencies can be determined by combining inequality (51) with equation (32)

$$|\sigma| \geqslant M(K, \mu), \qquad M(K, \mu) \equiv \sqrt{\left(\mu_R^2 / K^2 + 1\right)\left(\mu_I^2 - K^2\right)}.$$

The parameter μ^M that produces the required filtration when substituted into $\Lambda^{\text{Novikov}}_{\mu^M(\varphi)}$ is obtained by substituting $\rho = \mu_R \mu_I / K$ into equation (30) which results in the value $\mu^M = \mu_R \mu_I / K + \mathrm{i}K$. To summarize, we define μ^M as follows:

$$\mu^M = \begin{cases} \mu, & |\mu_I| \leqslant K \\ \mu_R \mu_I / K + \mathrm{i}K, & |\mu_I| > K. \end{cases} \tag{52}$$

In order to simplify analysis and computations, we will only consider a subset of the reconstructed frequencies defined by inequality

$$|\sigma| \geqslant |\mu_I| \sqrt{1 + \mu_R^2 / K^2}. \tag{53}$$

In other words, in order to guarantee stability of computations we need to exclude a disc of frequencies with the radius proportional to $|\mu_I|$. We further note that if trajectory is not circular but $|\theta(\varphi)| \leqslant \theta_0$, use of the cut-off $\mu^M = \mu_R(\theta_0)\mu_I(\theta_0)/K + \mathrm{i}K$ still results in a stable reconstruction of frequencies outside the disc of radius $|\mu_I(\theta_0)| \sqrt{1 + \mu_R^2(\theta_0) / K^2}$.

6. 3D reconstruction from closed-orbit measurements

We are now in a position to complete the development of the analytic procedure for the 3D SPECT reconstruction from parallel-beam data acquired from closed 1D paths. From

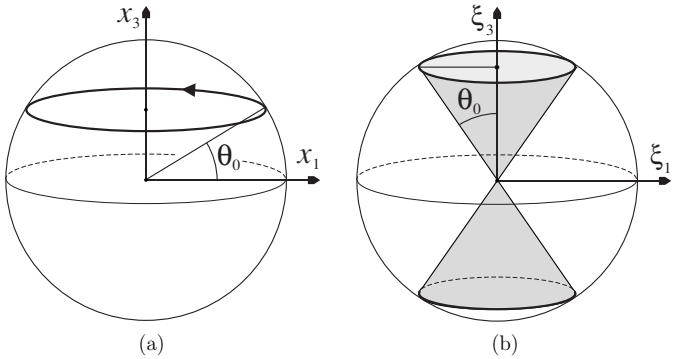

Figure 3. (a) Two-circle acquisition trajectory. (b) Cone of inaccessible frequencies.

the theoretical point of view, the solution to this problem has already been given in the previous sections. Indeed, in order to reconstruct the spatial activity distribution $F(\mathbf{r})$ from its 3D exponential Radon transform $G^{\mathrm{ERT}}(p, \varphi, x_3)$ (see equation (2)) it is enough to (i) compute the 1D Fourier transform $g(p, \varphi, \xi_3)$ (equation (7)), (ii) find $f(\mathbf{x}, \xi_3)$ for each value of parameter ξ_3 by evaluating either of the inversion formulae (16), (21) and (iii) compute $F(\mathbf{r})$ by a set of the 1D inverse Fourier transforms (4). However, stability of numerical implementation of these theoretically exact formulae cannot be guaranteed in general. In what follows we first analyse the stability of the reconstruction from measurements described by a circular orbit of directions. Then, in section 6.2 we describe an algorithm that permits stable reconstruction from two closed orbits satisfying certain conditions. A numerical example of such a reconstruction is presented.

6.1. Data measured from one circular orbit

First, let us consider the case of constant angle $\theta = \theta_0$, $\varphi \in [0, 2\pi]$. Then the directions of measurement are represented by the circle C on $\mathbb{S}^2$, with radius $\cos\theta_0$ (see figure 3(a)). Obviously, if $\theta_0 \neq 0$, there are great circles on $\mathbb{S}^2$ that do not intersect C. Therefore, Orlov's condition is not satisfied, and, in the absence of attenuation, the reconstruction is not possible, according to [10]. This statement seems to contradict the results of the previous sections which contain explicit reconstruction formulae valid under rather general conditions.

Let us try to reconcile these two points of view. Orlov's statement is based on the fact that (in the absence of attenuation) the 2D Fourier transform of a projection coincides (up to a constant factor) with a restriction of the 3D Fourier transform $\hat{F}(\xi)$ of the function $F(\mathbf{r})$ to a plane $\xi \cdot \tau = 0$ passing through the origin and perpendicular to the measurement direction $\tau(\varphi, \theta)$. Therefore, from a single projection one can reconstruct values of $\hat{F}(\xi)$ on that plane. In the simplest case when θ is constant and φ varies from 0 to 2π, the values of $\hat{F}(\xi)$ will be recovered for all ξ lying in the exterior of the cone Q_0,

$$Q_0 = \left\{\xi \,\middle|\, \xi_3^2 \geqslant \left(\xi_1^2 + \xi_2^2\right) \left|\cot\theta_0\right|\right\}$$

where subscript 0 in Q_0 indicates the absence of attenuation. While from the theoretical point of view it is possible to reconstruct $\hat{F}(\xi)$ for $\xi \in Q_0$ due to analyticity of $\hat{F}(\xi)$, such an analytic continuation is highly unstable and is impossible to implement numerically.

In turn, a closer look at the filtration operator $\Lambda^{\mathrm{present}}_{\mu(\varphi)}$ (equation (17)) reveals that it utilizes the values of the Fourier transform computed for complex values of the frequency z with $\max(|\mathrm{Im}\, z|) = |\mu_I| = |\xi_3 \tan\theta_0|$ (see equation (8)). Such a shift of the frequency in the

imaginary direction leads to instability of computations; this instability increases exponentially with the growth of ξ_3. (The same problem arises if one uses $\Lambda^{\text{Novikov}}_{\mu(\varphi)}$ instead of $\Lambda^{\text{present}}_{\mu(\varphi)}$.) This type of instability is closely related, for example, to the well-known instability of computation of the Laplace transform. Of course, some amount of instability is expected from problems of SPECT reconstruction. Indeed, in the simplest case when $\theta = 0$ and attenuation is purely real, there is still a shift of frequencies in the imaginary direction, as can be seen from equation (28). This shift leads to the well-known heightened noise sensitivity of the Tretiak–Metz inversion formula. Note, however, that in the latter case the shift is bounded. In our case the shift grows with the growth of ξ_3, rendering reconstruction of $F(\mathbf{r})$ practically impossible for this type of measurement, in spite of the existence of the explicit reconstruction formulae.

However, it is possible to reconstruct from one-circle measurement, in a stable fashion, spatial frequencies lying outside a certain cone in the frequency space. Indeed, as follows from the consideration of the previous section, the composition of the conventional weighted backprojection with the operator $\Lambda^{\text{Novikov}}_{\mu^M(\varphi)}$, where μ^M is defined by equation (52), leads to correct reconstruction of frequencies lying outside the disc of radius $|\mu_I|\sqrt{\left(\mu_R^2/K^2+1\right)}$. In turn, $|\mu_I| = |\xi_3 \tan\theta_0|$. The components of 2D frequency variable ζ from the previous section can be identified with the first two components of the 3D frequency variable ξ, i.e.,

$$\zeta_1 = \xi_1, \qquad \zeta_2 = \xi_2.$$

Thus using the filtration parameter μ^M, we reconstruct spatial frequencies satisfying the inequality

$$\sqrt{\xi_1^2+\xi_2^2}| \geqslant |\xi_3 \tan\theta_0|\sqrt{\mu_R^2/K^2+1}.$$

When this algorithm is used as a part of the 3D reconstruction, the frequencies outside the cone $Q_K = \left\{\xi \,||\xi_3| \geqslant |\cot\theta_0|\sqrt{\xi_1^2+\xi_2^2}/\sqrt{\mu_R^2/K^2+1}\right\}$ will be correctly reconstructed, with the imaginary shift remaining bounded by K.

Conversely, if it is desirable to reconstruct all frequencies in the exterior of a given cone Q defined by the equation

$$Q = \left\{\xi \,||\xi_3| \geqslant \sqrt{\xi_1^2+\xi_2^2}|\cot\theta^{\text{cutoff}}|\right\},$$

where angle θ^{cutoff} is given, the relation between the admissible direction angle θ_0 and the value of the shift K takes the form

$$\cot\theta^{\text{cutoff}} \leqslant \cot\theta_0/\sqrt{\mu_R^2/K^2+1}$$

or, equivalently,

$$\theta_0(K,\theta^{\text{cutoff}}) \leqslant \arctan\left(\frac{1}{\sqrt{\mu_R^2/K^2+1}}\tan\theta^{\text{cutoff}}\right). \tag{54}$$

For example, in the next section we will need to reconstruct frequencies outside the cone with the angle $\theta^{\text{cutoff}} = 45^\circ$. It follows from the inequality (54), that if K is chosen to equal μ_R, the measurement angle θ_0 can be as large as $\arctan(1/\sqrt{2}) \approx 35.264^\circ$. If a larger value of K (and a larger noise sensitivity of the algorithm) can be tolerated, then a larger angle θ_0 can be used. For example, if K is equal to $2\mu_R$, angle θ_0 can be increased to 41.81°, and so on. By choosing K large enough one can make angle θ_0 be arbitrarily close to θ^{cutoff} while keeping the imaginary shift bound by a constant K for all values of ξ_3.

To summarize, the 3D reconstruction problems with and without attenuation turn out to be quite similar. In both cases reconstruction of the spatial frequencies in the interior of the

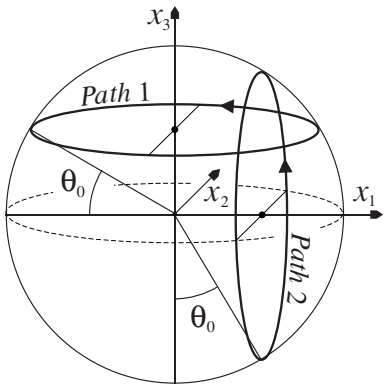

Figure 4. Two-circle acquisition trajectory.

prohibited cone is extremely (exponentially) unstable, in spite the fact that in the attenuated case we have a formal explicit representation for the solution of the problem. In the exterior of the cone reconstruction is possible; by using the filtration technique discussed in this section one can avoid exponential instabilities associated with progressive shifting of the frequencies in the imaginary direction.

In conclusion, we would like to note that from measurements corresponding to a wider non-circular trajectory $\theta = \theta(\varphi)$ such that $|\theta(\varphi)| \leqslant \theta_0$, one can reconstruct at least the same (possibly wider) range of frequencies than that reconstructed with $\theta = \theta_0$.

6.2. Data measured from two circular orbits

As demonstrated in the previous section, from one closed orbit one can reconstruct, in a stable fashion, only spatial frequencies of a function that lie outside a certain cone. One way to obtain a full reconstruction is to utilize a second trajectory of measurements supplying those frequencies that cannot be reconstructed from the first orbit.

An example of such a set of measurements is the two-circle path, consisting of two intersecting circles of directions with centres defined by two perpendicular vectors, as shown in figure 4. A simple reconstruction algorithm suitable for the two-circle measurements is presented below.

The method discussed in the previous section allows one to recover, from a circular trajectory $\theta(\varphi) = \theta_0$ with $\theta_0 < 45^\circ$, all frequencies $\hat{F}(\xi)$ for ξ lying outside the cone $Q^{(1)}_{45^\circ} = \left\{\xi \,|\, \xi_3^2 \geqslant \left(\xi_1^2 + \xi_2^2\right)\right\}$. Similarly, if the circle of directions is rotated by 90°, one can compute all frequencies outside the cone $Q^{(2)}_{45^\circ} = \left\{\xi \,|\, \xi_1^2 \geqslant \left(\xi_2^2 + \xi_3^2\right)\right\}$. Clearly, the union of the exteriors of these two cones contains all of $\mathbb{R}^3$:

$$\mathbb{R}^3 \subseteq \left(\mathbb{R}^3 \setminus Q^{(1)}_{45^\circ}\right) \cup \left(\mathbb{R}^3 \setminus Q^{(2)}_{45^\circ}\right).$$

Combining the two sets of frequencies corresponding to each of the circles would be quite straightforward in a frequency domain algorithm, for example in the method based on circular harmonics formulae of section 5.2. (Algorithms of this sort usually require accurate interpolations between grids in the spectral domain, and the design of such methods is not a trivial task.) For the FBP-type algorithm presented here, we choose a different approach. For each of the circular paths, we will reconstruct a function with a missing 90° wedge of frequencies (instead of a function lacking a certain cone of frequencies). This can be achieved

by additional filtration of function $f(\mathbf{x}, \xi_3)$ in $\mathbf{x}$ for each value of ξ_3. We will thus obtain from the data corresponding to the first circular trajectory, a function $F_1(\mathbf{r})$ with such Fourier transform $\hat{F}_1(\xi)$ that

$$\hat{F}_1(\xi) = \begin{cases} \hat{F}(\xi), & |\xi_3| < |\xi_1| \\ \frac{1}{2}\hat{F}(\xi), & |\xi_3| = |\xi_1| \\ 0, & |\xi_3| > |\xi_1|. \end{cases}$$

Similarly, from the second trajectory we recover function $F_2(\mathbf{r})$ such that

$$\hat{F}_2(\xi) = \begin{cases} \hat{F}(\xi), & |\xi_3| > |\xi_1| \\ \frac{1}{2}\hat{F}(\xi), & |\xi_3| = |\xi_1| \\ 0, & |\xi_3| < |\xi_1|. \end{cases}$$

Obviously, the sum of $F_1(\mathbf{r})$ and $F_2(\mathbf{r})$ yields the sought function $F(\mathbf{r})$.

In detail, the first part of the algorithm consists of

- computing $g(p, \varphi, \xi_3)$, equation (7) for the first set of data,
- setting $\theta^{\text{cutoff}} = 45^\circ$ and finding the smallest value of the constant K satisfying inequality (54),
- for each value of ξ_3:
  - (i) setting $\mu_I = \xi_3 \tan\theta_0$,
  - (ii) choosing μ^M according to equation (52),
  - (iii) reconstructing $f_1^M(\mathbf{x}, \xi_3) = \left(B_\mu \Lambda_{\mu^M}^{\text{Novikov}} g(p, \varphi, \xi_3)\right)(\mathbf{x}, \xi_3)$,
  - (iv) filtering $f_1^M(\mathbf{x}, \xi_3)$

$$f_1^{\text{filtered}}(\mathbf{x}, \xi_3) = \mathcal{F}_2^{-1}\left[h(\xi, \xi_3)\hat{f}_1^M(\xi, \xi_3)\right](\mathbf{x}, \xi_3)$$

  with a filter $h(\xi_1, \xi_3)$ such as

$$h(\xi_1, \xi_3) = \begin{cases} 1, & |\xi_1| > |\xi_3| \\ \frac{1}{2}, & |\xi_1| = |\xi_3| \\ 0, & |\xi_1| < |\xi_3|, \end{cases}$$

- and, finally, reconstructing $F_1(\mathbf{r})$ through the inverse 1D Fourier transform of $f_1^{\text{filtered}}(\mathbf{x}, \xi_3)$:

$$F_1(\mathbf{r}) = F_1^*(\mathbf{x}, x_3) = \frac{1}{\sqrt{2\pi}} \int_{\mathbb{R}} f_1^{\text{filtered}}(\mathbf{x}, \xi_3)\, \mathrm{e}^{\mathrm{i}x_3\xi_3}\, \mathrm{d}\xi_3.$$

Computation of $F_2(\mathbf{r})$ is done by rotating the coordinate system and applying the same algorithm as was used to reconstruct $F_1(\mathbf{r})$. Finally, $F(\mathbf{r})$ is obtained as a sum of $F_1(\mathbf{r})$ and $F_2(\mathbf{r})$.

The above algorithm can also be used, without any changes, for reconstruction from two orbits of more general shape, such that the first orbit satisfies the condition $|\theta^{(1)}(\varphi)| \leqslant \theta_0$, and the second trajectory satisfies the similar condition $|\theta^{(2)}(\varphi)| \leqslant \theta_0$ (in the rotated coordinate system).

It is easy to give an approximate asymptotic estimate of the number of floating point operations required for this method. Assume for simplicity that the number of projections equals n, the dimension of data in one projection is $n \times n$, and the image is reconstructed on a $n \times n \times n$ 3D Cartesian grid. Since a 2D FBP algorithm requires $O(n^3)$ floating point operations, and there are $O(n)$ spatial slices in discretization in ξ_3, the total number of required operations is $O(n^4)$.

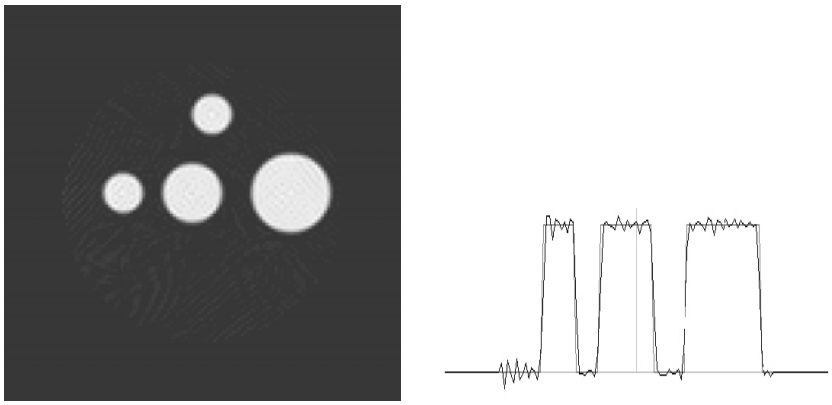

(a) (b)

Figure 5. Reconstructed image: (a) activity in the plane $\xi_2 = 0$ and (b) comparison of the reconstructed activity on the line $\xi_2 = 0, \xi_3 = 0$ with the exact values.

Table 1. Parameters of the model functions.

j	$c_x^{(j)}$	$c_y^{(j)}$	$c_z^{(j)}$	R_j
1	0.45	0.0	0.05	0.20
2	−0.05	0.0	0.05	0.15
3	−0.40	0.0	0.05	0.10
4	−0.05	0.4	0.05	0.15
5	0.05	0.0	0.45	0.10

6.2.1. Numerical example. In this section, we present an example of image reconstruction from data measured from the two-circle orbit, described by equation $\theta_0 = 35^\circ$ (in the original and rotated coordinates) and shown in figure 4. In the present test the model activity distribution was given by a sum of five characteristic functions $\chi(\mathbf{c}^{(j)}, R_j)$ of spheres with centres $\mathbf{c}^{(j)}$ and of radius R_j:

$$F(\mathbf{r}) = \sum_{j=1}^{5} \chi(\mathbf{c}^{(j)}, R_j),$$

with the values of the parameters chosen as shown in table 1.

The reconstruction was performed in the region $|\mathbf{r}| \leqslant 1/\sqrt{2}$, and the (physical) attenuation ν was set to 3. The total optical diameter of the domain was equal to $3\sqrt{2} \approx 4.24$. Under such a combination of parameters the reconstruction problem is equivalent to that for an object of 35 cm in diameter in the presence of realistic attenuation of 12 cm^{-1}. A total of 800 projections were modelled (400 for each circular path); each projection was of the size 129×129. The unit cube in the reconstruction domain was mapped onto a $129 \times 129 \times 129$ Cartesian grid; however, the actual computations were restricted to the sphere of radius $1/\sqrt{2}$. The computation took 21.5 min on a PC with AMD Athlon 1600+ processor.

The result of the reconstruction is shown in figure 5. Part (a) of the figure demonstrates the section of the 3D image by the plane $y = 0$. The graph of the activity along the line $y = 0$, $z = 0$ is shown in figure 5(b), with the graph of the original function on the background.

7. Conclusions

We have shown that the problem of the 3D reconstruction from attenuated parallel-beam measurements can be reduced to a set of the 2D AD-ERTs with complex-valued attenuation. Explicit formulae were presented for inversion of such transforms. One of our formulae are of the FBP type, while the other is based on decomposition in cylindrical harmonics in the angular variable. We have proved these formulae by a rather elementary approach based on the Cauchy theorem in 1D variable. It was also shown that the simple substitution of the complex-valued attenuation into the Kuchment–Shneiberg formula (in a slightly modified form) also leads to correct FBP-type reconstruction.

The proposed set of explicit reconstruction formulae for the solution of the original 3D problem is theoretically valid for any closed set of measurement directions. A simple analysis shows, however, that in general, only a certain cone of frequencies can be reconstructed from measurements whose direction are described by one closed trajectory.

On the other hand, if two sets of measurements are available such that frequencies that cannot be obtained from one set are available from the other, a stable reconstruction is possible. We showed that the two partial reconstructions can be combined if one recovers a certain wedge of frequencies from one set, and a complimentary wedge of frequencies from the other one.

As an example, we presented a reconstruction algorithm and obtained a satisfactory reconstruction for the two-circle trajectory satisfying certain conditions. The proposed algorithm can be applied, without any changes to a more general trajectory consisting of two closed orbits, provided that these two orbits are wider than the circles in our example (i.e., angle $\theta(\varphi)$ is smaller than or equal in absolute value to θ_0). A similar approach can be used to combine more partial reconstructions obtained from more than two sets of closed-orbit measurements, provided that the union of the wedges of frequencies that can be recovered from each orbit covers all of $\mathbb{R}^3$.

The algorithm we developed is intended to serve as a 'proof of the idea' rather than a ready-to-use reconstruction technique. The noise sensitivity of this method (as presented) is similar to the noise sensitivity of the original Tretiak–Metz formula. The practical application of such methods is impeded by a significant level of noise present in experimentally measured data. More advanced, stable analytical techniques in the case of constant attenuation usually (although not necessarily) involve cylindrical harmonic decomposition allowing one to filter out unstable harmonics (see [13] and references therein for a unified analysis of such techniques). A similar technique can be utilized to design a stable circular reconstruction algorithm for the case of AD-ERT, based on the results of section 5.2 (see, in particular, the discussion at the end of that section). Moreover, it is desirable to combine such a technique with the fast FFT-based methods employing interpolations in the spectral domain. Such methods, well studied in the context of x-ray tomography (see, for example, [20–24]), yield full 3D reconstructions in just $O(n^3 \log n)$ floating point operations, which is important in view of significant volume of data describing 3D images. However, a detailed design of such a more advanced, stable and fast numerical algorithm is outside of the scope of this paper.

Finally, we would like to compare the present algorithm to the methods of [4, 6] from the point of view of practical reconstruction. The latter techniques require computation of the composition of the inverse classical and exponential Radon transforms (or two exponential Radon transforms) each of which is an ill-posed inverse problems. In contrast, the present method combines a set of the inverse exponential Radon transforms with the numerically stable Fourier transform, which, we believe is advantageous. On the other hand, the methods of [4, 6] seem to be more flexible and, at least at present, they allow one to treat a wider set

of trajectories. For example, it is not clear currently how to modify our approach to treat elongated trajectories, such as the one given by

$$\theta(\varphi) = \frac{\pi}{2}\sin^2\varphi - 0.1$$

although this orbit does satisfy Orlov's condition and can be processed using the methods of [6].

Acknowledgments

We gratefully acknowledge support by the NSF, through grant DMS-0312292. The author would like to thank P Kuchment, H Barrett and R Clackdoyle for valuable discussions, and to express gratitude to both the anonymous referees for multiple suggestions and comments that helped to significantly improve this paper.

Appendix

In this appendix, we show that if $u(z)$ is a finitely supported continuous function with a bounded piece-wise continuous derivative, then the expression $\hat{u}(z)\,\mathrm{e}^{\mathrm{i}pz}[z - \mathrm{i}A]$ vanishes in the limit $\mathrm{Re}\,z \to +\infty$ uniformly in $y = \mathrm{Im}\,z$ within the strip $0 \leqslant y \leqslant B$, where p and A are arbitrary real numbers and B is an arbitrary positive number. In other words, we would like to prove that for any $\varepsilon_0 > 0$ there exists $R_0 > 0$ such that $|\hat{u}(z)\,\mathrm{e}^{\mathrm{i}pz}[z - \mathrm{i}A]| < \varepsilon_0$ for all $z = x + \mathrm{i}y$ such that $x > R_0$ and $0 \leqslant y \leqslant B$.

Without loss of generality it is enough to consider the case $A = 0$, $p = 0$, i.e., it is sufficient to prove that $|\mathrm{i}z\hat{u}(z)| < \varepsilon_0$. For a fixed y, the expression $\mathrm{i}z\hat{u}(z)$ is the Fourier transform of the function $\frac{\mathrm{d}}{\mathrm{d}p}(u(p)\,\mathrm{e}^{yp})$

$$\begin{aligned}\mathrm{i}(x+\mathrm{i}y)\hat{u}(x+\mathrm{i}y) &= \frac{\mathrm{i}(x+\mathrm{i}y)}{\sqrt{2\pi}}\int u(p)\,\mathrm{e}^{-\mathrm{i}p(x+\mathrm{i}y)}\,\mathrm{d}p\\ &= \frac{1}{\sqrt{2\pi}}\int u'(p)\,\mathrm{e}^{-\mathrm{i}p(x+\mathrm{i}y)}\,\mathrm{d}p\\ &= \frac{1}{\sqrt{2\pi}}\int (u(p)\,\mathrm{e}^{yp})'\,\mathrm{e}^{-\mathrm{i}px}\,\mathrm{d}p.\end{aligned}$$

By the well-known Riemann–Lebesgue theorem [25], since $\frac{\mathrm{d}}{\mathrm{d}p}(u(p)\,\mathrm{e}^{yp})$ is a bounded piece-wise continuous function, its Fourier transform vanishes in the limit $x \to \infty$. Therefore, for a fixed $\mathrm{Im}\,z = y$, $\forall\varepsilon > 0$ there exists $R(y) > 0$ such that $|z\hat{u}(z)| < \varepsilon$ when $\mathrm{Re}\,z > R(y)$. In other words, $z\hat{u}(z)$ goes to zero as z goes to infinity along any of the lines $y = \mathrm{Im}\,z = \text{const}$. However, for our purposes we need to prove that such convergence is uniform in y within the strip $0 \leqslant y \leqslant B$.

Pick $R_1 = \max(R(B), R(0))$. Then $|z\hat{u}(z)| < \varepsilon$ for $x > R_1$, $y \in \{0, B\}$. Consider harmonic function $v(z) = \mathrm{Re}(z\hat{u}(z))$. It can be represented as a sum $v(z) = v_1(z) + v_2(z)$ of two harmonic functions each of which is a solution of the Dirichlet problem in a half strip S defined by inequalities $0 < \mathrm{Re}\,z < B$, $x > 0$, with the following boundary conditions:

$$v_1(z) = \begin{cases} v(z), & z \in \partial S, \quad \mathrm{Re}\,z < R_1,\\ 0, & z \in \partial S, \quad \mathrm{Re}\,z \geqslant R_1,\end{cases}$$

$$v_2(z) = \begin{cases} v(z), & z \in \partial S, \quad \mathrm{Re}\,z \geqslant R_1,\\ 0, & z \in \partial S, \quad \mathrm{Re}\,z < R_1.\end{cases}$$

Since $|v(z)| < \varepsilon$ when $\operatorname{Re} z > R_1$, by the maximum principle $|v_2(z)| < \varepsilon$ within the half-strip. In the half-strip $S_1 = \{z | x > R_1, 0 < y < B\}$ function $v_1(z)$ can be represented by the following series:

$$v_1(z) = \sum_{k=1}^{\infty} C_k \exp\left(-\frac{\pi k(x - R_1)}{B}\right) \sin\frac{\pi k y}{B}$$

with $|C_k| \to 0$ as $k \to \infty$. For $x > R_1$, the following estimate holds:

$$\begin{aligned} |v_1(z)| &\leqslant \max|C_k| \sum_{k=1}^{\infty} \exp\left(-\frac{\pi k(x - R_1)}{B}\right) \\ &= \max|C_k| \exp\left(-\frac{\pi(x - R_1)}{B}\right) \frac{1}{1 - \exp\left(-\frac{\pi(x-R_1)}{B}\right)}. \end{aligned}$$

As $x \to \infty$, the latter expression converges to 0. Therefore, $\exists R_2 > R_1$ such that $|v_1(z)| < \varepsilon$ for $x > R_2$. Hence, $|\operatorname{Re}(z\hat{u}(z))| = |v(z)| < 2\varepsilon$ for $x > R_2$. Similarly, $\exists R_3 > R_1$ such that $|\operatorname{Im}(z\hat{u}(z))| < 2\varepsilon$. Therefore for $x > R_0 = \max(R_2, R_3)$, we obtain $|z\hat{u}(z)| < 2\sqrt{2}\varepsilon$. Selecting $\varepsilon = \frac{\varepsilon_0}{2\sqrt{2}}$ completes the proof of the claim made in the beginning of this section.

Similarly, one can prove the uniform convergence of $|z\hat{u}(z)|$ to zero within the strip $-B < \operatorname{Re} z < 0, x < 0$ in the limit $x \to -\infty$.

References

[1] Noo F, Clackdoyle R and Wagner J-M 2002 Inversion of the 3D exponential x-ray transform for a half equatorial band and other semi-circular geometries *Phys. Med. Biol.* **47** 2727–35

[2] Palamodov V P 1996 An inversion method for an attenuated x-ray transform *Inverse Problems* **12** 717–29

[3] Wagner J-M and Noo F 2001 Three-dimensional image reconstruction from exponential parallel-beam projections *IEEE Trans. Nucl. Sci.* **48** 743–9

[4] Wagner J-M, Noo F and Clackdoyle R 2002 Exact inversion of the exponential x-ray transform for rotating slant-hole (RSH) SPECT *Phys. Med. Biol.* **47** 2713–26

[5] Wagner J-M, Noo F, Clackdoyle R, Bal G and Christian P 2003 Attenuation correction for rotating slant-hole (RSH) SPECT using exact rebinning *IEEE Trans. Nucl. Sci.* **50** 110–6

[6] Wagner J-M 2002 Methodes analytiques pour la correction d'attenuation en tomographie tridimensionnelle par emission monophotonique *Collection des Publications de la Faculte des Sciences Appliquees, PhD Dissertation* University of Liege, Belgium

[7] Markoe A 1984 Fourier inversion of the attenuated x-ray transform *SIAM J. Math. Anal.* **15** 718–22

[8] Mennessier C, Noo F, Clack R, Bal G and Desbat L 1999 Attenuation correction in SPECT using consistency conditions for the exponential ray transform *Phys. Med. Biol.* **44** 2483–510

[9] Kuchment P and Shneiberg I 1994 Some inversion formulae in the single photon emission computed tomography *Appl. Anal.* **53** 221–31

[10] Orlov S S 1975 Theory of three dimensional reconstruction: 1. Conditions of a complete set of projections *Sov. Phys. Crystallogr.* **20** 312–4

[11] Bellini S, Piacentini M, Cafforio C and Rocca F 1979 Compensation of tissue absorption in emission tomography *IEEE Trans. Acoust. Speech Signal Process.* **27** 213–8

[12] Tretiak O J and Metz C 1980 The exponential Radon transform *SIAM J. Appl. Math.* **39** 341–54

[13] Metz C E and Pan X 1995 A unified analysis of exact methods of inverting the 2D exponential Radon transform, with implications for noise control in SPECT *IEEE Trans. Med. Imag.* **14** 643–58

[14] Arbuzov E V, Bukhgeim A L and Kazantsev S G 1998 Two-dimensional tomography problems and the theory of *A*-analytic functions *Siberian Adv. Math.* **8** 1–20

[15] Novikov R G 2002 An inversion formula for the attenuated x-ray transformation *Ark. Mat.* **40** 145–67

[16] Kunyansky L A 2001 A new SPECT reconstruction algorithm based on the Novikov's explicit inversion formula *Inverse Problems* **17** 293–306

[17] Hawkins W G, Leichner P K and Yang N C 1988 The circular harmonic transform for SPECT reconstruction and boundary conditions on the Fourier transform of the sinogram *IEEE Trans. Med. Imag.* **7** 135–48

[18] Inouye T, Kose K and Hasegawa A 1989 Image reconstruction algorithm for single-photon-emission computed tomography with uniform attenuation *Phys. Med. Biol.* **34** 299–304

[19] Shneiberg I, Ponomarev I, Dmitrichenko V and Kalashnikov S 1994 On a new reconstruction algorithm in emission tomography *Applied Aspects of Radon Transform* ed S Gindikin (*AMS Transl*. vol 162) (New York: Am. Math. Soc.) pp 247–55
[20] Natterer F 1986 *The Mathematics of Computerized Tomography* (New York: Wiley)
[21] Potts D and Steidl G 2001 A new linogram algorithm for computerized tomography *IMA J. Numer. Anal*. **3** 769–82
[22] Axelsson C and Danielsson P E 1994 Three-dimensional reconstruction from cone-beam data in $\mathcal{O}(N^3 \log N)$ time *Phys. Med. Biol*. **3** 477–91
[23] Schaller S, Flohr T and Steffen P 1998 An efficient Fourier method for 3D Radon inversion in exact cone-beam CT reconstruction *IEEE Trans. Med. Imag*. **2** 244–50
[24] Basu S and Bresler Y 2002 $\mathcal{O}(N^3 \log N)$ backprojection algorithm for the 3D Radon transform *IEEE Trans. Med. Imag*. **2** 76–88
[25] Titchmarsh E C 1948 *Introduction to the Theory of Fourier Integrals* (Oxford: Clarendon)